Medical Image Processing by using Soft Computing Methods and Information Fusion

HARITON COSTIN[1, 2] and CRISTIAN ROTARIU[1]
(1) Faculty of Medical Bioengineering
'Gr.T. Popa' University of Medicine and Pharmacy, Iaşi
9-13, Kogalniceanu str., 700454, Iaşi
(2) Institute of Computer Science of Romanian Academy Iaşi Branch
ROMANIA
E-mail: hcostin@gmail.com
http://www.iit.tuiasi.ro/personal/h_costin.html

Abstract: - Medical images are increasingly being used within healthcare for diagnosis, planning treatment, guiding treatment and monitoring disease progression. Technically, medical imaging mainly processes uncertain, missing, ambiguous, complementary, inconsistent, redundant contradictory, distorted data and information has a strong structural character. As a general approach, the understanding of any image involves the matching of features extracted from the image with pre-stored models. The production of a high-level symbolic model requires the representation of knowledge about the objects to be modeled, their relationships, and how and when to use the information stored within the model.

This paper reports new (semi)automated methods for the segmentation and classification of medical images using soft computing techniques (e.g. fuzzy logic, neural networks, genetic algorithms), information fusion and specific domain knowledge. Fuzzy logic acts as a unified framework for representing and processing both numerical and symbolic information ("hybridization"), as well as structural information constituted mainly by spatial relationships in biomedical imaging. Promising results show the superiority of the soft computing and knowledge-based approach over best traditional techniques in terms of segmentation errors. The classification of different anatomic structures is made by implementing rules yielded both by domain literature and by medical experts. Though the proposed methodology has been implemented and successfully used for model-driven in the domain of medical imaging, the deployed methods are generic and applicable to any structure that can be defined by expert knowledge and morphological image analysis.

Key-Words: - medical image processing, artificial intelligence, soft-computing, knowledge-based processing, data fusion.

1 Introduction

Artificial Intelligence has proved to yield promising results in digital image processing and analysis when missing, ambiguous or distorted data is available. Moreover, for biomedical image analysis the structural character of information may successfully be approached by using methods of A.I.: Knowledge Based Systems, Expert Systems, Decision Support Systems, Neural Networks, Fuzzy Logic and Systems, Neuro-Fuzzy Systems, Evolutionary and Genetic Algorithms, Data Mining, Knowledge Discovery, Semantic Nets, Symbolic Calculus for knowledge representation, etc. The *data fusion* methods successfully solve the aggregation of numerical and linguistic information, and are able to cope with ambiguous, uncertain, conflicting, complementary, imprecise and redundant information, like that occurring in biomedical imaging domain, in order to provide a more accurate and less uncertain interpretation.

In fact, all main stages of a pattern recognition process (i.e. image pre-processing/enhancement, segmentation, features selection, pattern classification) may have their soft computing approaches and it depends only on actual applications if these approaches are used or not.

Clinical applications imply at least an adaptability capability performed through a knowledge-based / decision-making system, a soft-computing method or a non-linear technique [26].

The specific big complexity in medical imaging is based on huge amounts of data, large knowledge

bases, incompleteness, imprecision, noise, inconsistency in data and knowledge (a definite lack for good models in many areas of medicine), redundancy, various ways of reasoning, including qualitative reasoning, heuristics, and subjective reasoning [24].

Soft computing (*SC*) methods (fuzzy logic [13], genetic algorithms [15] and neural networks [14][18]), that include both qualitative and quantitative representations, fill the gap between the needs of the medical science and traditional modeling and inference methods in precise sciences [4][6][7][8][12][21][28]. The final stage of data sources processing is to combine the available information to derive the best data and/or decision through data fusion methods [19].

The main medical domains in which SC finds challenging applications are diagnosis, treatment, rehabilitation, prevention, screening, surgery, and healthcare management. These applications go from "classical" ones (e.g. electrocardiogram interpretation) to automated diagnosis, medical knowledge discovery, medical image bases management, intelligent techniques in rehabilitation, etc.

SC methods for medical imaging and data fusion straighten their application in clinical medicine, e.g. in radiation therapy, general surgery, conventional neurosurgery, etc.

Data fusion facilitates a better use of image data by providing methods for the fusion of data from multiple modalities, e.g. multimodal registration and fusion between anatomical and functional data, the fusion of data from different patients or with a priori knowledge (models and/or atlases) and the recognition of complex anatomical structures and their symbolic identifications, when they are not explicitly described by the image contents. As medical imaging is strongly domain-dependent, three aspects of data fusion are of particular emphasis on brain imaging, for instance. The first one concerns the combination of images and/or generic data; specifically, methods for multimodality registration and matching of data from different individuals by means of warping models. The second aspect concerns the identification of anatomical structures. Finally, data hybridization for 3D display techniques to render the combined data is useful for user interface.

In the following we have approached the topic through two applications of SC in medical image processing and analysis.

2 Knowledge – Based Contour Detection using Fuzzy Logic and Knowledge Representation

The use of fuzzy logic and semantic knowledge for edge detection and segmentation of magnetic resonance (MR) images of the brain [9], [10], [11], shown the superiority of the knowledge-based approach over best traditional techniques in terms of segmentation errors. Our method uses:

- a fuzzy knowledge-based contour detection technique;
- a semantic net for representing domain knowledge;
- robust contour detection by searching of an optimal path between two known points of the contour that optimizes a cost function, by means of a breadth-first graph search strategy.

Image *segmentation* is one of the most important steps leading to the analysis of digital images, its main goal being to divide an image into disjoint parts that have a strong correlation with objects or areas of the real world [1][3][5][16][23]. Among the low-level segmentation methods, there are two different approaches. The first involves *region-based segmentation*: classification by thresholding, looking for sets of attributes, region growing, division and merging. The second approach involves *contour-based segmentation* (looking for local discontinuities): derivatives operators, active contours (snakes), mathematical morphology, etc. These two groups of methods solve a dual problem, in the sense that each region can be represented by its closed boundary, and each closed boundary describes a region. The region adjacency graph is a usual example of this duality. But these methods often lead to missing edge pieces (gaps) or ambiguities if no domain specific knowledge about the expected contours is incorporated. Because of the different natures of the various edge- and region-based techniques, they may be expected to give somewhat different results/information and consequently the segmentation itself is not unique. Contours in biomedical imaging have a fuzzy nature due to: (i) greyness ambiguity, arising from the contrast inhomogeneity of identical anatomical objects; (ii) spatial ambiguity, coming from variations in size, shape, position and pathological variability; (iii) partial volume effects, i.e. the image of two tissues in one voxel (or pixel). Therefore, exact decisions about the location of contour points are in principle impossible, but "best estimate" decisions can be made, as physicians do when

ISBN: 978-1-61804-011-4

interactively defining the outlines of anatomical structures (regions of interest-ROI).

Fuzzy Iconic Level. A two-dimensional (2D) fuzzy image $FI_{M,N}$ is a 2D real function f(x, y) defined on each pixel coordinate (x, y) so that $0 \le x < M$, $0 \le y < N$ and $0 \le f(x, y) \le 1$. The fuzzy image reflects some specific properties, e.g. brightness, edginess and texture, that are defined by the *membership function f*(*x,y*). The membership function has often a triangular form. As alternatives, fuzzy logic uses specific nonlinear functions, such as Z, S, or Π. So, a fuzzy image is the projection of a digital image by a membership function. If more fuzzy images are assigned to one single 2D image, then the fuzzy image is represented by a 3D image whose third dimension is defined by the number of fuzzy images:

$$f_i(x, y) : I_{M,N} \rightarrow FI^{i}_{MxN} ; f_i(x, y) \in [0, 1]; i \in \{1, 2, \ldots, K\} \quad (1)$$

where K indicates the number of possessed properties. Figure 1 shows a typical fuzzy image processing procedure.

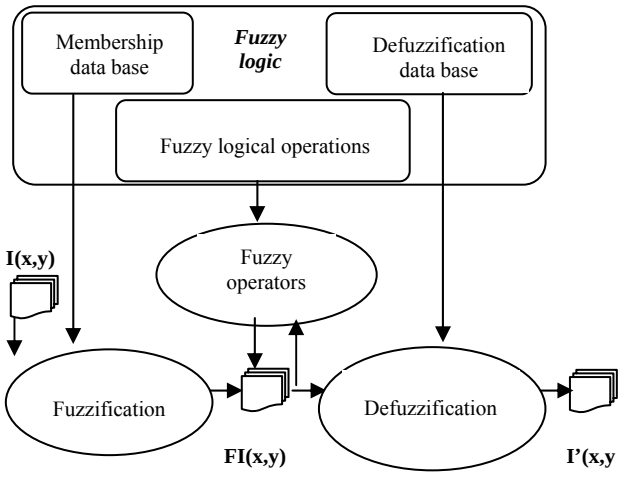

Fig. 1. Diagram of typical fuzzy image processing

The objective of our contour-based segmentation procedure is the detection of fuzzy contour of objects, in which "fuzzy" does not refer to the shape of contours but to their representation mechanism. The image sets are labeled with contour names (e.g. background/skin). Each set member is assigned a value on [0, l] representing its grade of membership for a contour. Fuzzy sets are in function notation with image point vectors as arguments.

$$f_{contour\_name} : [0 \ldots N]^2 \rightarrow [0, 1], \quad 0 \le f_{contour\_name} \le 1, \quad (2)$$

where N refers to the image size. The contours are represented in frames, which comprise parametrical and relational knowledge for each desired contour. Fuzzy sets for each contour are calculated collecting evidence by means of well defined operationalizations of knowledge in the frames. Some methods for operationalization are described below.

(a) Gradient

Evidence for a contour is its high grey value gradient. So, with the assertion "The *Background/Skin* contour has a *high gradient* in the ρ image" and $|g_\rho(x)|$ is the magnitude of the gradient of ρ, normalized to the interval [0, l], we follow that

$$f_{background/skin}(x) \le \left| g_\rho(x) \right|. \quad (3)$$

We use "≤" as the conjunction of the above assertion and all other assertions about this specific contour should be used to define the fuzzy set for the contour. A conjunction is expressed by a *minimum* operation in fuzzy logic. Of course, the initial value of each fuzzy set value should be one, as no assertion can increase fuzzy values.

(b) Direction

As long as we are dealing with convex objects, we may employ valuable information using direction of the gradient. We define a center c_ρ of our images and a direction vector d_ρ, depending on *x*.

$$c_\rho = \frac{\sum x\rho(x)}{\sum \rho(x)}, \quad d(x) = c_\rho - x \cdot \quad (4)$$

The assertion "The *direction* of the ρ gradient is *inside* for the *Background/Skin* contour" can be operationalized with unit vectors g'_ρ and d'_ρ:

$$f_{background/skin}(x) \le N_{pos}\left(g'_\rho(x) \cdot d'_\rho(x)\right). \quad (5)$$

N_{pos} is a normalization function that maps all negative values to 0 and normalizes all positive values linearly to the interval [0, 1]. The constraint function is proportional to the angle between the gradient and d_ρ. If the direction is *outside*, d_ρ is used with opposite sign.

(c) Relations

In addition, we may also use relations among contours. With an assertion like "The *background/skin* contour is *outside* the skin/bone contour" we may say that $f_{background/skin}(x)$ must not exceed the largest value of $f_{skin/bone}$ along a line between *x* and c_ρ:

$$f_{background/skin}(x) \le N_d \max_{0 \le \lambda \le 1}\left(f_{skin/bone}(x + \lambda\, d_\rho(x))\right) \quad (6)$$

N_d is again a normalization factor, which is determined for each d to map values on [0, 1]. If the maximum-term is very low, there is a low plausibility for the $f_{skin/bone}$ contour *inside* point x and therefore a low plausibility for x being *outside* of $f_{skin/bone}$.

Similarly, *inside* can be defined as

$$f_{bone/brain}(x) \le N_d \max_{\lambda \le 0}\left(f_{skin/bone}(x + \lambda\, d_\rho(x)\right). \quad (7)$$

Knowledge representation. We used these methods of operationalization in conjunction with a suitable knowledge representation technique for four contours in our magnetic resonance images (in brackets we quote the image on which the procedure is applied): *background/skin(ρ), skin/bone(ρ), bone/brain(ρ)* and *brain/ventricles*(T_1). The frame representations of knowledge about these contours are:

background/skin:	*skin/bone:*
has-a-high-gradient-in : ρ	has-a-high-gradient-in: ρ
gradient-direction-is: inside, ρ	gradient-direction-is: outside, ρ
is-outside-of : skin/bone	

bone/brain:	*brain/ventricles:*
has-a-high-gradient-in: ρ	has-a-high-gradient-in: T_1
gradient-direction-is : inside, ρ	gradient-direction-is: inside, T_1
is-inside-of : skin/bone	is-inside-of: bone/brain

As can be seen, the slot *gradient-direction-is* has two values, one giving the direction and the other referring to the gradient image to be used.

All fuzzy sets for contours are initialized with 1 for each pixel and each pixel has the highest membership value for each contour. The assertions represented in the above slots of each contour frame are implemented using the operationalization of knowledge. Relational assertions can be used only if the argument (the value of, e.g., *is-outside-of*) is a frame with no slots that have not been applied. That is, one can use a contour as argument of relational assertions of other contours if all knowledge has already been applied. The algorithm for knowledge application is simple, but practical situations lead to complex representations.

Robust contour detection. As traditional edge detectors applied to fuzzy contours yield unwanted gaps, we approached this task as a search of an optimal path between two known points of the contour that optimizes a cost function, by using a *breadth-first graph search* strategy. Four initial points acting both as starting point and end point of different contour segments were chosen. The result is a closed border made by four contour segments.

The procedure starts from c_ρ (4), searches for initial points in the four directions π/4 separated, and selects the points having the maximal product of $|g_\rho(x)|$ and fuzzy contour values for each.

To each image pixel four features are attached: (i) $\Phi(x) = arctg\,(g_x(x)/g_y(x))$, gradient direction; (ii) $|g(x)|$, gradient magnitude; (iii) $\Phi_C(x) = \Phi(x) + \pi/2$, contour direction·(mod π); (iv) $f_{contourname}(x)$, fuzzy contour values. The transfer *cost function* for each possible contour point is defined as

$$C(x, x') = (C_1(x, x') + w\, C_2(x, x'))\, f(x'), \quad (8)$$

x and x' being two neighboring points with x' a candidate successor of x and w a weight. The terms of (8) are as follows:

$$C_1(x, x') = \Delta_g(x, x') = |g(x') - g(x)| + |g(x') - g(x_{end})| \quad (9)$$

with x_{end} the predefined contour end point. This term assures local continuity when referring to gradient values.

$$C_2(x,x') = \Delta_\alpha(x,x') = [|\Phi_C(x) - \alpha(x,x')| + |\Phi_C(x') - \alpha(x,x')|] / 2, \quad (10)$$

with α denoting the direction of (x-x') line. $C_2(x)$ is upper bounded by a threshold value, θ_α, whose exceeding sets C_2 to infinity. Both terms capture small global variations of gradient and assure early quit of paths with high costs. This cost function favors smooth contours and small deviations of the path direction α from the contour direction $\Phi_C(x)$.

The term $f(x')$ in (8) is defined as

$$f(x') = 2 - f_{contourname}(x') \quad (11)$$

and it comes from the knowledge-based contour detection phase.

The search algorithm begins at a certain start point as root node. Each node is expanded according to its 8 neighbors if transfer cost does not equal infinity and contains the cumulative cost and a link to its predecessor. The breadth-first graph search technique implies the simultaneous expanding of all nodes with the same number of predecessors, till the end point is reached. After all nodes with low transfer costs have been expanded, the optimal contour is found by tracing the nodes from x_{end} back to x_{start} along the predecessor path. At each point an estimate of the costs to x_{end} is added as a heuristic term. For lowering the number of graph nodes, at each level this number is limited to the best n nodes.

ISBN: 978-1-61804-011-4

Results. We used experimentally the following values for tuning the cost function: w=0.70 in (8), $\theta_\alpha = 70^0$. n=30 nodes were used for graph search procedure.

Results of the contour detection for the images in Figure 2 are displayed in Figures 3, 4 and 5, respectively. In order to assess the effectiveness of fuzzy contour detection, a comparison with two traditional edge detection methods (Sobel and Canny operators [23]) has been shown. In our study only little knowledge about the desired contour was used.

Figure 5 presents a ρ-weighted image of a brain with tumor. One can observe its low contrast, which is a severe impediment for traditional edge detection techniques. In comparison with the very popular Canny filter our method yields superior results concerning the accuracy of edge detection. Figure 6 shows segmentation results obtained by using model knowledge and semantic networks. Thus, *ventricles* from T_1-image (Figure 2b), the *tumor* from "Tumor"-image and the imagistic fuzzy set *inside(bone)* with contours superposed were obtained after a short processing time.

Another advantage of the use of iconic fuzzy sets is that they partially overcomes the problems of image preprocessing (contrast normalization, histogram equalization, filtering a.s.o.), which must be used with traditional techniques when we are faced with low/variable contrast and noisy images.

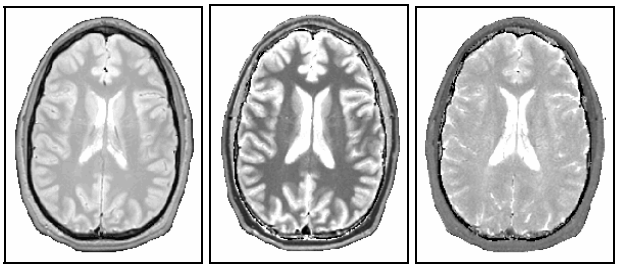

(a) *ρ image* (b) *T1 image* (c) *T2 image*

Fig. 2. ρ, T1 and T2 images of an axial MRI section

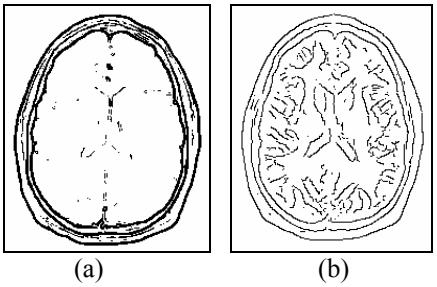

(a) (b)

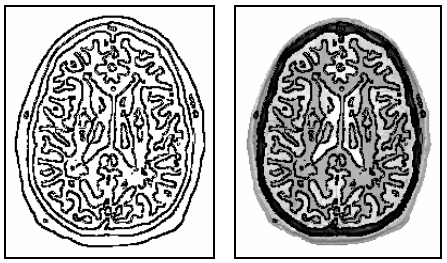

(c) (d)

Fig. 3. ρ image: Sobel (a); Canny (b); fuzzy contour (c); (c) and Figure 2(a) superposed (d)

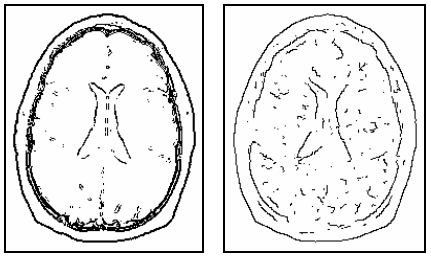

(a) (b)

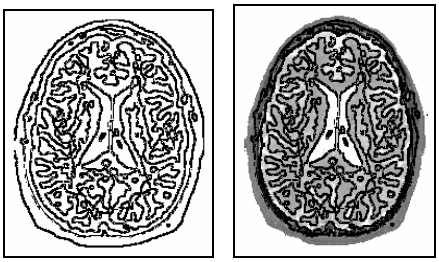

(c) (d)

Fig. 4: T_2 image: Sobel (a); Canny (b); fuzzy contour (c); Fig.(c) and Fig.2(c) superposed (d)

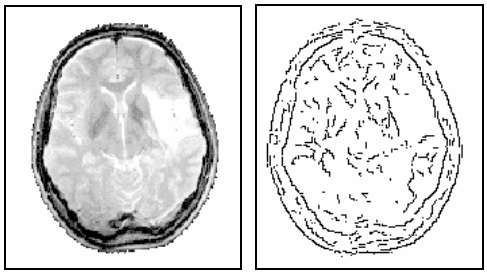

(a) (b)

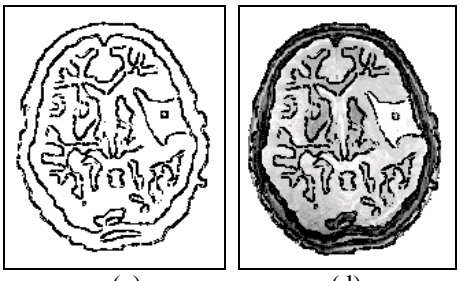

(c) (d)

Fig. 5. "Tumor" image (a); Canny (b); fuzzy (c); figures (a)+(c) superposed (d)

ISBN: 978-1-61804-011-4

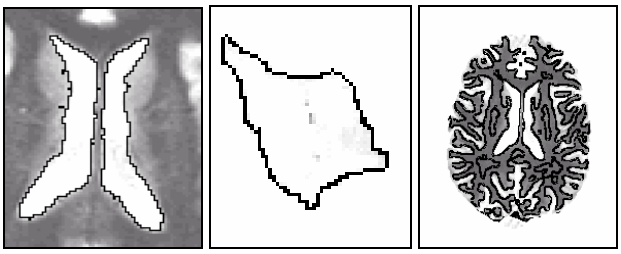

(a) (b) (c)

Fig. 6. Ventricles from T_1 image (a); tumor from "Tumor" image (b); *inside*(*Bone*) from T_1 (c)

3 Contour-Based Image Segmentation using Genetic Algorithms

We have developed a semi-automated contour-based segmentation method in which first the domain expert manually traces different contours of objects of interest. Then, these contours are used as a training data set for a contour tracking method based on an elastic-contour model, optimized by a genetic algorithm.

The experiments were made both on synthetic images and on real CT images of the brain, interpreted by medical experts from the Neurosurgery Hospital in Iasi, Romania.

3.1 Elastic contour model

A classic segmentation method [20] represents the contour to be tracked as a deformable curve, also called "snake", whose shape is finally determined by different forces and external constraints. Each force acts along the direction of the scan line to which its start edge point belongs. The amplitude of these forces is computed from image features. A pseudo-energy functional, that contains both internal energy of the curve and those forces that attract the curve towards the contour to be detected, is defined.

The best contours are represented by the lowest energy values, so the segmentation task becomes the optimization problem to minimize the energy function given by the formula

$$E = \int_0^1 \left(E_{\text{int}}(v(s)) + E_{img}(v(s)) + E_{con}(v(s))\right) ds \ , \quad (12)$$

where $v(s) = (x(s), y(s))$ is the parametric equation of the curve, E_{int} is the internal energy of the „snake", E_{img} accounts for forces yielded by image parameters, and E_{con} stands for external constraints.

The internal energy is given by

$$E_{\text{int}} = \frac{\alpha(s)\left|dv(s)/ds\right|^2 + \beta(s)\left|d^2v(s)/ds^2\right|}{2}, \quad (13)$$

where $\alpha(s)$ and $\beta(s)$ are two parameters.

The attractive field generated by image edges is

$$E_{\text{img}} = w_l E_l + w_m E_m + w_{term} E_{term} \ , \quad (14)$$

where w_l , w_m şi w_{term} are weights chosen by the user. The function used for E_l is the intensity (brightness) of the image: $E_l = I(x, y)$.

The term that acts for attracting curve by the edges is given by

$$E_m = -\left|\nabla I(x,y)\right|^2 . \quad (15)$$

E_{term} takes into account segment ends and corners and is given by

$$E_{term} = \frac{I^s_{xx}(I^s_x)^2 - 2I^s_{xy}I^s_xI^s_y + I^s_{xx}(I^s_y)^2}{\left[(I^s_x)^2 + (I^s_y)^2\right]^{\frac{3}{2}}}, \quad (16)$$

where $I^s(x, y) = G_\sigma(x, y) * I(x, y)$ is the convolution of $I(x, y)$ with a Gaussian kernel and the terms in (16) are obtained by deriving the gradient angle $\arctan(I^s_x / I^s_y)$ with respect to the unit vector, normal to the gradient direction.

The „discrete" formula of the total energy (12) is

$$E_d = \sum_{i=1}^{n} E_{\text{int}}(i) + E_{img}(i) + E_{con}(i) , \quad (17)$$

where the sum of the last two terms is called E_{ext}.

By passing to finite differences, we may write for the internal energy

$$E_{\text{int}}(i) = \alpha_i \frac{\left|v_i - v_{i-1}\right|^2}{2h^2} + \beta_i \frac{\left|v_{i-1} - 2v_i + v_{i+1}\right|^2}{2h^4} . \quad (18)$$

The optimization condition implies the deriving the total energy and equaling it to zero. This operation yields in matrix notation

$$\mathbf{Ax} + \mathbf{f}_x(\mathbf{x}, \mathbf{y}) = 0 \quad (19)$$

$$\mathbf{Ay} + \mathbf{f}_y(\mathbf{x}, \mathbf{y}) = 0 ,$$

where $\mathbf{A}$ is a penta-diagonal matrix and $\mathbf{f}_x(i) = (dE_{ext}/dx_i)$, $\mathbf{f}_y(i) = (dE_{ext}/dy_i)$.

Solving the above equation system determines the coordinates $\mathbf{x}$ and $\mathbf{y}$ of each contour pixel. The fully-automated method needs a seed contour placed near the desired local minimum of energy to prevent it to be caught by other possible minima, so some knowledge brought by the user and semi-automated approach are more than appropriate.

ISBN: 978-1-61804-011-4

3.2 Designing the contour detection optimized by genetic algorithms

Our contour tracking method uses two stages:
(1) *a non-linear contour detector*;
(2) an *interpolation block* based on „snake" model.

As the overall precision depends on both these modules, a genetic algorithm (GA) achieves the global optimization. First, it acts on the training set of manually delineated contours and maximizes a fitness function that yields a value that represents the degree of similarity between the references and the contours in the input image. The set of edge points yielded by the contour detector is interpolated with an elastic model, the procedure is initiated by the training contours set, and then is applied to the whole input image.

The contour detector. A second-order polynomial filter is used for edge detection. The scan geometry (Fig. 7) shows that for each point $P_{h,k-1}$ of the contour C_{k-1} one defines the scan segment L_h, centered around $P_{h,k-1}$, that is S_w pixels in length, along the direction of the normal to C_{k-1} in $P_{h,k-1}$. Within this line of S_w pixels the input image is resampled.

The output of the filter, $o(x_i)$, for each point x_i and N_p filtering pixels, is given by

$$o(x_i) = c_0 + \sum_{k=1}^{N_p} c_k^{'} \cdot x_{i-d_K} + x_{i-d_K} \cdot \sum_{l=k}^{N_p} c_{k,l}^{''} \cdot x_{i-d_l} \ , \quad (20)$$

where c_0, $c_k^{'}$, $c_{k,l}^{''}$ (k, l=1, ..., N_p) are filter coefficients and d_k (k=1, ..., N_p) are the displacements along the scan line, with respect to x_i (i = 1, ..., S_w), of the N_p pixels. All the above parameters are optimized by the GA.

A threshold criterium will then select a subset of edge points x_i for which the value of $o(x_i)$ is greater than a value T, and all $o(x_i)$=1 for those samples.

3.3 Segmentation through contour detection optimized by genetic algorithms

Genetic algorithms are bio-inspired optimization methods that are capable to solve applications where deterministic techniques fail or in which the computing load is too high [2][15][17][22][27].

In our approach, for each line L_h the edge detector yields a set of points, $\{ X_i , i = 1,..., N(h) \}$, defined as $\{ x_j \in L_h \,|\, o(x_j) > 0, j = 1,..., S_w \}$. It is possible that in certain scan regions $N(h) = 0$ or $N(h) > 1$, thus the actual position of contour points being altered by noise. Now the elastic contour model and genetic optimization go into action.

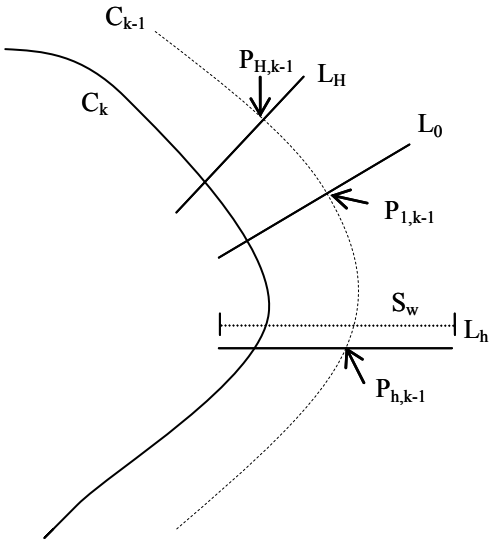

Fig. 7. Scan geometry for contour detection

Let us denote by $f_k(h)$, k=1, ..., $N(h)$ the coordinates of the contour points X_k extracted on the scan line L_h , and by $y(h)$ the coordinates of the contour point that must be detected. Thus, the contour $y(h)$ is the locus of points that minimize the energy functional (12), that may be rewritten as:

$$E(y) = \int_{[0,H]} \left(\left| y''(h) \right|^2 + \sum_{i=1}^{N(h)} \beta_i(h) \cdot p_i(h) \right) dh \, , \quad (21)$$

where $\beta_i(h)$ is the stiffness of the „spring" corresponding to the contour point $X_i(h)$. In formula (12) or (21) we consider E_{img} = 0, this treating the possible important variations in contour shape.

By using the above notations, we can define the fitness function used by the GA:

$$F(\{y\}) = K - \sqrt{\sum_{k=1}^{H} \left(y^r(k) - y(k) \right)^2} \, , \quad (22)$$

where $y^r(k)$ is the distance, along L_h, between the contour point belonging to the training contour and the origin of the reference system for L_h , that equals the corresponding edge point on L_{h-1} . K is a constant chosen so that $F(\{y\}) \geq 0$, and H is the number of reference contours.

4 Results

4.1 Tests on generated images

A 3D phantom object was generated, that can be software sectioned. In this manner pseudo-tomographic slices result, having a volume of 58368 voxels, a geometric resolution of 512x512 pixels

and a 8-bit grey scale. The region of interest is a 128x128 area.

First, to test the sensitivity to noise, a zero-mean gaussian noise with standard deviations of respectively 25 and 50, was added (Fig. 8). The test shown a good robustness to noise: the precision of contour detection significantly lowers only when σ>50 grey levels. The effectiveness of contour detection was computed as reconstruction error of the 3D object, based on its sections, whose mean value is less than 1,5% (see Table 1).

The tests with GA implementation were made using Matlab® programming environment, by means of *ga* function that allowed efficient computation of the fitness function.

Table 1. The estimated volume, cumulated error, percentage error and mean error for software-generated object and for real CT images

Noise level (σ)	$\hat{V}$	E	$E\%$	$\overline{E}$
0	58826	425	0,78	10,11
25	59037	873	1,13	20,78
50	59258	1429	**1,5**	34,02
CT images	9571	687	**3,11**	16,35

The above parameters are defined as follows:

(1) $\hat{V} = \sum \hat{V}_k$,where $\hat{V}_k$ is the estimated object area on the k 2D-slice; so, $\hat{V}$ is the total estimated volume;

(2) if $\Delta V_i = \hat{V}_i - V_i$, with V_i being the real object area in section i, then $E = \sum |\Delta V_i|$ (total cumulated error);

(3) $E\% = 100 \cdot (\frac{\sum V_i}{\sum \hat{V}_i} - 1)$ (percentage error);

(4) $\overline{E} = E / H$ (absolute mean error).

4.2 Tests on real CT images

The tests evaluated both quantitatively and qualitatively the quality of contour tracking. In this case the training process was made using fewer images than in the case of artificial objects.

Yet, the mean error of the contour detection was under 5% for very „clean" images (S/N ratio ≥ 50dB). Thus, our approach based on elastic contour and genetic optimization was successfully verified. Moreover, the low reconstruction errors obey a zero-mean distribution. This fact also illustrates the „fuzzy" character of contours delineation in CT cerebral images, when noise often occurs, and the partial volume effect is present in 3D tomographic reconstruction too, due to the thickness of the used planar sections.

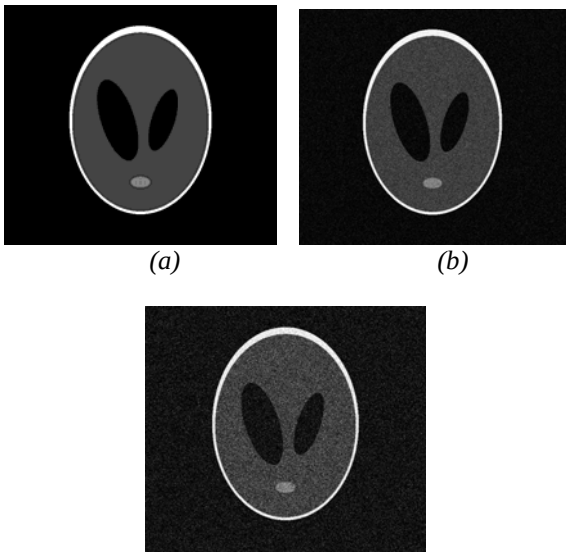

(a) *(b)*

(c)

Fig. 8. O software-generated section: noiseless (a) and with gaussian noise [(σ = 25 in (b) and σ = 50 in (c)]

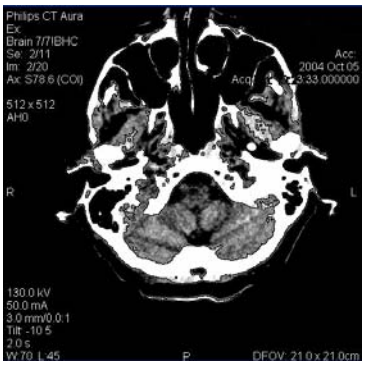

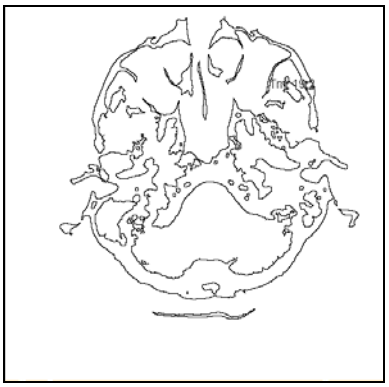

Fig. 9. Contour detection on a CT image using „snake" model and GA optimization

5 Clinical Applications of Image Segmentation and Registration

5.1 Planning Surgery of the Brain and Skull Base

In neurosurgery, the structure of interest delineation and the combination of MR and CT images of the head (the so called *registration* procedure) can be useful in planning certain types of neurosurgical procedures, as the relationship between the soft tissue contrast provided by MRI and bone details provided by CT can be useful when a single modality is insufficient. The clinical motivation of good contour detection and registration stage is to provide the surgeon with an improved understanding of the relationship among the lesion, adjacent critical structures, and possible surgical approaches. This can result in better positioning of craniotomies, reduced craniotomy size, and quicker operations with less time under anesthetic.

5.2 Localizing Electrodes in the Brain

Functional neurosurgical procedures include implantation of electrodes over the surface of the brain or depth electrodes into brain parenchyma to localize an epileptogenic region or focus by subsequent neurophysiological recording in patients with intractable epilepsy. This is done to plan surgical resection of the epileptogenic area of the brain, so good anatomical localization of the electrode is crucial for the success of the operation. Another type of functional neurosurgical procedure is the implantation of electrodes into the subthalamic nucleus in patients with Parkinson's disease, to alleviate tremor.

5.3 Radiotherapy Planning

The recent development of 3D CT-based radiotherapy planning has involved the use of multiple CT slices to show a tumor in all three dimensions. This allows "conformal" radiotherapy to be planned, where multiple radiation beams are used, configured as tightly as possible to the contour of a tumor to spare adjacent potentially radiosensitive normal tissues from damage. This technique has been of most use in the head and skull base and to preserve brain and optic nerves, and has also been applied to the prostate. MR images seem ideal for the purposes of planning, as the much greater soft tissue contrast of MR allows better definition of the boundaries of a tumor from adjacent normal tissues and structures.

In the brain, MR techniques such as functional studies or perfusion imaging can also provide information about eloquent areas of the brain that would have significant consequences for the patient if damaged, or the physiology of an already treated tumor, which may influence whether further treatment is required. When a tumor is irradiated, the margins of the radiation beams carefully and precisely calculated on the planning images must correspond exactly spatially to the beams used to irradiate the patient. The images used for planning purposes must be geometrically accurate. But MR is subject to distortions to a greater extent than CT. Moreover, CT has a further important advantage over MR: the intensities of image voxels (measured in Hounsfield units) represent electron density and can be used to calculate dose distributions directly. These two factors have limited the use of MR scans so far for radiotherapy planning.

In this respect, the precise segmentation of the anatomic structures of interest is crucial for a successful radiotherapy procedure. Also, the registration of CT and MR images provides one way to overcome the imagistic problems in neurosurgery, as utilizing different information from both modalities can enhance treatment.

Acknowledgment

The author would like to thank my colleague, Prof. dr. Ion Poeată, both for the help in manually segmentation of the used images of the brain, and for results evaluation during our experiments.

References:

[1] Acharya, R., Menon, R.P.: A Review of Biomedical Image Segmentation, in Singh, A., Goldgof, D., Terzopoulos, D. (eds.), *Deformable Models in Medical Image Analysis*, IEEE Computer Society Press, Los Alamitos, Ca., 1998, 140-161.

[2] Banu, B., Lee S., Ming, S: Adaptive Image Segmentation using a Genetic Algorithm, *IEEE Trans. on SMC*, Vol. 25, No.12, 1995, 1543-1568.

[3] Bovik, Al (ed.): *Handbook of Image and Video Processing*, Academic Press, 2000.

[4] Comaniciu, D., Meer, P., Foran, D.: Image-Guided Decision Support System for Pathology, *Machine Vision And Applications*, Springer-Verlag,1999, 11: 213–224.

[5] Costin, H.: *Image Processing and Analysis. Applications In Biomedical Imaging*, Tehnica Info Publ. House, Kisinev, 2004.

[6] Costin, H., *et. al*.: 3D Reconstruction from Serial Fine Sections of Rat Brain Using Neural Networks and a Genetic Algorithm, *Proc. of The World Congress on Medical Physics and Biomedical Engineering*, Chicago, 2000.

[7] Costin H., Rotariu Cr.: Tremor Assessment by Means of Handscript Analysis and Fuzzy Logic, *Biomedical Soft Computing and Human Sciences Journal*, Japan, **7**, No. 1, 2001 39-45.

[8] Costin, H., Rotariu, Cr., et al.: Fuzzy Rule-Aided Decision Support for Blood Cell Recognition, *Journal of Fuzzy Systems and Artificial Intelligence*, Romanian Academy, Bucharest, Vol. 7, Nr.1-3, 2001, 61-70.

[9] Costin, H., Boiculese, L., et al., Biomedical Image Segmentation Using Semantic Networks and Imagistic Fuzzy Sets, *Proc. of ECIT2002*, European Conference on Intelligent Technologies, Iasi, Romania, 2002 (on CD).

[10] Costin, H., Rotariu, Cr., Biomedical Image Analysis by Means of Soft-Computing and Semantic Networks, *Proc. of EMBEC´02*, 2nd European Medical & Biological Engineering Conference, Vienna (2002) 1574-1575.

[11] H. Costin, Cr. Rotariu: Knowledge-Based Contour Detection in Medical Imaging Using Fuzzy Logic, *Proc. of SCS 2003*, Int. IEEE Conf. on Signals, Circuits, Systems, Iaşi, Romania, 2003, 273-276.

[12] H. Costin, Biomedical Image Processing and Analysis via Artificial Intelligence and Information Fusion, book chapter in: *Knowledge Based Intelligent Systems for Health Care*, T. Ichimura and K. Yoshida (Eds.), Advanced Knowledge Int. Publ. House, Australia, 2004, pp. 121-160

[13] Dubois D., Prade H., Yager R. (eds.): *Readings in Fuzzy Sets for Intelligent Systems*, Morgan Kaufmann Publ., 1993.

[14] Dumitrescu, D., Costin, H.: *Neural Networks. Theory and Applications*, Teora Publ. House, Bucharest, 1996 (in Romanian).

[15] Goldberg, D.E.: *Genetic Algorithms in Search, Optimization & Machine Learning*, Addison-Wesley, 1989.

[16] Gonzales, R.C., Woods, R.E.: *Digital Image Processing*, 2nd Ed., Prentice Hall, 2002.

[17] Hall, L.O., Ozyurt, I.B., Bezdek, J.C.: Clustering with a Genetically Optimized Approach, *IEEE Transactions on Evolutionary Computation*, Vol. 3, No. 2, 1999, 103-112.

[18] Haykin, S.: *Neural Networks*, Prentice-Hall, 1994.

[19] Jain, L.C., Martin, N.M.: *Fusion of Neural Networks, Fuzzy Systems and Genetic Algorithms: Industrial Applications*, CRC Press, 1998.

[20] Kass, M., Witkin, A., Terzopoulos, D.: Snakes: Active Contour Models, *Int. Journal of Computer Vision*, Vol. 1, 1987, pp. 321-331.

[21] Kobashi, S., et al.: Fuzzy Cluster Analysis for MR Angiography Image Classification, Proc. Iizuka '98, Japan (1998), 329-332.

[22] Pignalberi, G., et al.: Tuning Range Image Segmentation by Genetic Algorithm, *EURASIP Journal of Applied Signal Processing*, No.8, 2003, 780-790.

[23] Pratt, W.K.: *Digital Image Processing*, (3rd ed.), John Wiley & Sons, New York, (2001).

[24] Sonka M., Hlavac V., Boyle R.: *Image Processing, Analysis and Machine Vision* (2nd ed.), PWS Publishing, 1999.

[25] Vial, S., Gibon, D., Vasseur, C., Rousseau, J.: Volume Delineation by Fusion of Fuzzy Sets Obtained From Multiplanar Tomographic Images, *IEEE Trans. on Medical Imaging*, Vol. 20, No. 12, 2001, 1362-1372.

[26] Teodorescu, H.N., Kandel, A., Jain, L.C. (Eds.): *Fuzzy and Neuro-Fuzzy Systems in Medicine*, CRC Press, Boca Raton, London, New York, 1999.

[27] Yoshimura, M., Oe, S.: Evolutionary Segmentation and Multiresolution Analysis of Texture Image using Genetic Algorithms and 2D Wavelet Decomposition, *Proc. Iizuka '98*, Japan, 1998, 987-991.

[28] Zhang, M., Hall, L., Goldgof, D.: A Generic Knowledge-Guided Image Segmentation and Labeling System Using Fuzzy Clustering Algorithms, *IEEE Transactions on Systems, Man, and Cybernetics*, Part B, V.32, No.5, 2002, 571-582.